IEEE Access
Multidisciplinary | Rapid Review | Open Access Journal

Received February 21, 2020, accepted March 11, 2020, date of publication March 16, 2020, date of current version March 26, 2020.

Digital Object Identifier 10.1109/ACCESS.2020.2980926

An Analytical Scalable Lumped-Element Model for GaN on Si Inductors

MARIO SAN MIGUEL MONTESDEOCA[1,2], SERGIO MATEOS ANGULO[1,2], DANIEL MAYOR DUARTE[1,2], JAVIER DEL PINO[2], (Member, IEEE), JAVIER A. GARCÍA Y GARCÍA[2], (Member, IEEE), AND SUNIL L. KHEMCHANDANI[2], (Member, IEEE)

[1]Wireless Innovative MMIC (WIMMIC), 35004 Las Palmas de Gran Canaria, Spain
[2]Institute for Applied Microelectronics (IUMA), University of Las Palmas de Gran Canaria, 35017 Las Palmas de Gran Canaria, Spain

Corresponding author: Mario San Miguel Montesdeoca (mario.sanmiguel@wimmic.com)

This work was supported in part by the Spanish Ministry of Science, Innovation and Universities under Grant RTI2018-099189-B-C22, and in part by the Canary Agency for Research, Innovation and Information Society (ACIISI), Canary Islands Government under Grant ProID2017010067.

ABSTRACT In this paper, a wide-band distributed model that can approximate the behaviour of square and octagonal inductors, both with and without tapering, is presented. This paper also presents a novel way of accurately modelling the lateral coupling in the substrate. The presented model can be applied to any foundry process, and its validity has been demonstrated using a novel technology, the D01GH GaN process developed by OMMIC, which has a high resistivity substrate. To do so, seventeen inductors have been designed and manufactured. The proposed model has been verified against EM simulations and measurements of the designed inductors. Comparisons show that the model can correctly estimate the behaviour of the inductor, improving the results of the EM simulations for most cases. The root mean square (RMS) error calculated across the samples when estimating the inductance is 0.0565. The RMS error for the quality factor results (2.2727) is also adequate, although there is more deviation when comparing the results with the measurements.

INDEX TERMS Inductor model, lateral coupling, octagonal inductor, square inductor, tapered inductor.

I. INTRODUCTION

Integrated inductors are a key component in RFIC and MMIC designs, since they have a significant impact on the size and performance of the overall system. Because of this, estimating the behaviour of these components has been a topic of interest for the integrated design community for the last two decades. Several works found in the literature provide different models and techniques to model the behaviour of manufactured inductors [1]–[4]. However, the growing interest in GaN processes in the last years has increased the need for a model that can correctly predict the behaviour of an inductor layed out on a high-resistivity substrate.

Additionally, an accurate model for tapered inductors would be welcome in the circuit designer community. Tapering is a well-known and widely discussed approach for increasing the quality factor (Q) of an inductor [5]–[7]. The quality factor of an inductor is the ratio of its reactance to its series resistance. The tapering technique consists on the gradual decrease of the width of each turn of the inductor so that the outer turns are wider, reducing the ohmic losses of the inductor, and the inner turns are narrower, maximising the magnetic field flowing through the inner hole of the inductor.

Numerous effects must be accounted for when modelling an inductor, especially a tapered one, such as DC inductance, skin effects, eddy currents and lateral coupling of the substrate. The first three effects have been widely analysed in the past [8]–[11]. [12] deems lateral coupling as not significant or negligible on high-resistivity substrates, like the ones on GaN or GaAs processes. Many papers have attempted to emulate the effect of lateral coupling using resistors and capacitors (R_M and C_M), but the calculation of their values has always been based on adjustment parameters or by applying extraction methods [13]–[16]. The model presented in this paper includes mathematical formulation for modelling lateral coupling and its impact on a high-resistivity substrate has been demonstrated.

This paper proposes a model that can be utilised to predict the behaviour of square and octagonal inductors, both

The associate editor coordinating the review of this manuscript and approving it for publication was Yue Zhang.

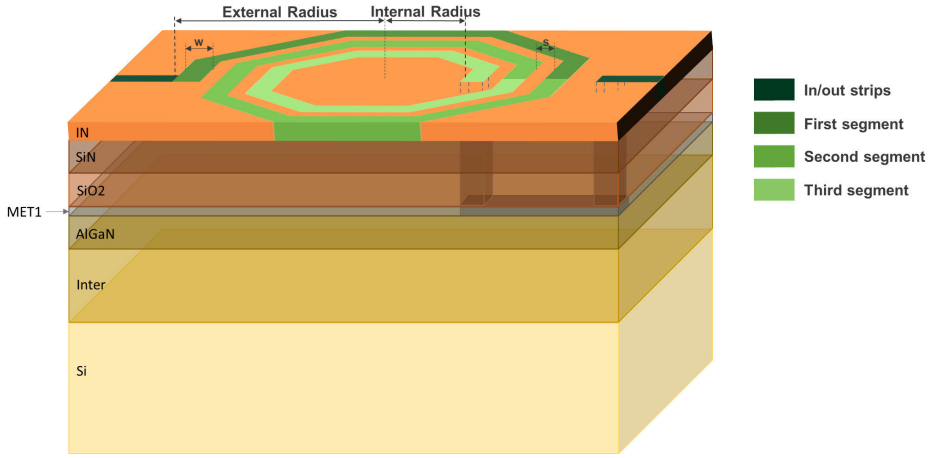

FIGURE 1. Generic inductor inset in the D01GH process.

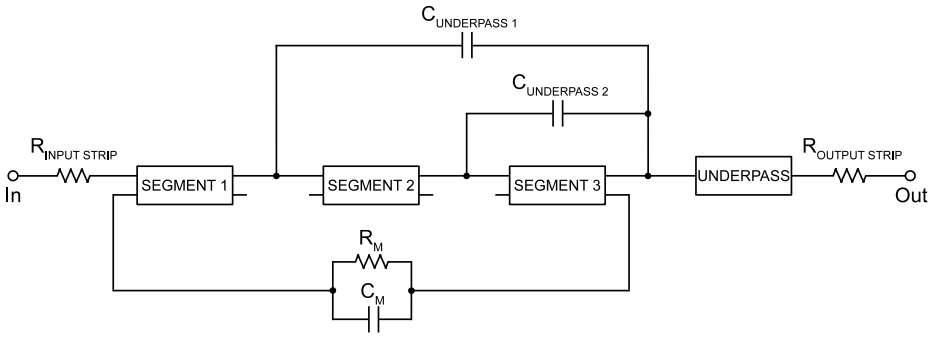

FIGURE 2. Proposed inductor model for the inductor shown in Fig.1.

tapered and non-tapered. The model and its equations are explained in Section II, whereas a comparison between the results of the model, electromagnetic (EM) simulations and measurements for different manufactured inductors is shown in Section III. Finally, some conclusions are drawn in Section IV.

II. PROPOSED INDUCTOR MODEL

The first aspect to consider when developing the model of an inductor is the different materials involved in the definition of the technology and their distribution. The D01GH GaN process developed by OMMIC follows a similar composition to other GaN on Si technologies. A simplified version of the cross-section for this process including an octagonal inductor is shown in Fig.1. In this case, the inductor is constructed on the IN metal layer. The underpass of the inductor is defined in the Metal 1 (MET1) layer. Between these metal layers are two additional layers, SiN and SiO_2, which act as dielectric materials. Under the MET1 layer, two high resistivity layers (AlGaN and Interface) can be found. Finally, the Silicon (Si) substrate occupies the bottom layer.

In addition to the utilised technology, several parameters have to be taken into account when developing the inductor model. Among these parameters are the shape of the inductor (square, octagonal, circular), its number of turns or segments, the length and width of each segment (important for the case of tapered inductors), the length and width of the underpass and the materials of the different metal layers that make up the inductor. Once these parameters have been properly defined, the equivalent inductor model shown in Fig.2 can be applied. In this scalable model, the number of segments is mainly defined by the number of turns of the inductor. Therefore, for an inductor with two turns, there will be two segments, whereas for an inductor with two and a half turns like the one shown in Fig.1, the number of segments will be three.

A. SEGMENT BLOCK MODELLING

The schematic for the Segment block of the model is shown in Fig.3. In this model, $R_{SKIN(i)}$ and $L_{(i)}$ represent the skin and proximity effects of the inductor [1], [8] [12] for the segment. The total DC inductance of the inductor is split evenly across the segments, while the resistance of each segment is calculated using (1) [1], where $l_{(i)}$ and $w_{(i)}$ are the length and

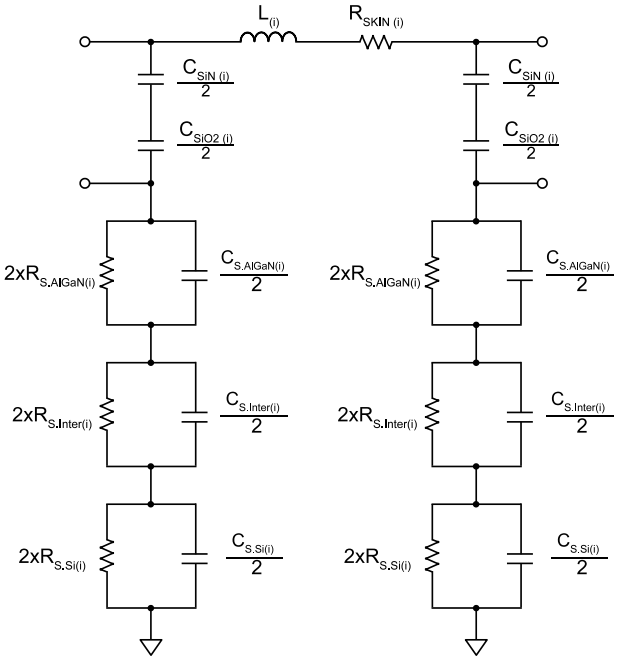

FIGURE 3. Schematic of the SEGMENT block.

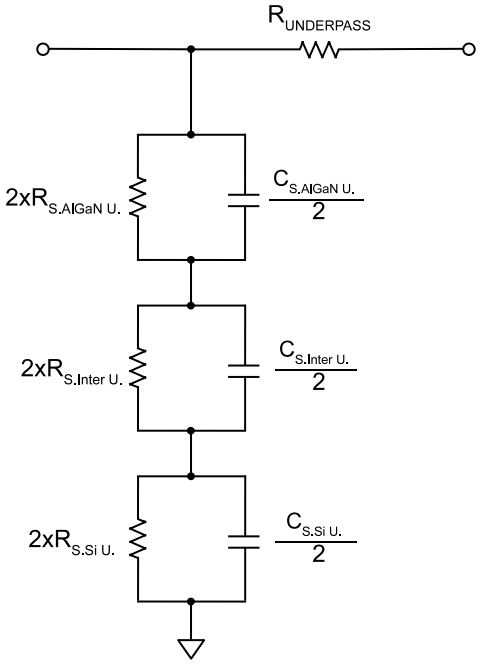

FIGURE 4. Schematic of the UNDERPASS block.

width of the segment, σ is the conductivity of the metal of the inductor (IN), t_{IN} is the thickness of said metal and δ_{EFF} is the effective skin depth, calculated using (2).

$$R_{SKIN(i)} = \left(\frac{l_{(i)}}{2 \cdot \sigma \cdot w_{(i)} \cdot \delta}\right) \cdot \left[\frac{sinh\left(\frac{t_{IN}}{\delta_{EFF}}\right) + sin\left(\frac{t_{IN}}{\delta_{EFF}}\right)}{cosh\left(\frac{t_{IN}}{\delta_{EFF}}\right) + cos\left(\frac{t_{IN}}{\delta_{EFF}}\right)}\right] \quad (1)$$

$$\delta_{EFF} = \sqrt[3]{\frac{t_{IN}}{w}} \cdot \delta = \sqrt[3]{\frac{t_{IN}}{w}} \cdot \sqrt{\frac{2}{\mu\sigma\omega_0}} \quad (2)$$

In (2), w is the maximum width of the inductor, μ is the magnetic permeability of the material and ω_0 is the angular frequency. In this model, it is assumed that the magnetic field is spread evenly across the substrate and that no elements are placed under the inductors. This is a common practice in MMIC design.

To properly model the substrate of the inductor, all the process layers should be considered in order to have the most accurate model possible. Thus, the capacitance of the SiN and SiO_2 layers under the IN metal area occupied by each segment ($A_{(i)}$) of the inductor had to be modelled. To do so, (3) and (4) are utilised, where t is the thickness of the material. The AlGaN, Inter and Si layers found below the MET1 layer are also considered. Since this process has a high resistivity substrate, where ρ_{Si} is 5k$\Omega\cdot$ cm and ρ_{AlGaN} and ρ_{Inter} are 100k$\Omega\cdot$ cm, the resistance of each of these layers must also be considered. The capacitances and resistances of each layer can be obtained by applying (5) and (6) [1], [17]. In these equations, $v = A_{(i)}/\pi$. The equations for the Inter and Si layers are the same as for AlGaN, but keeping in mind that the characteristics and properties (thickness, permitivity and resistivity) of each layer are different. Since this is a distributed model, the capacitors that account for the capacitance of each layer are divided by two, as it can be observed in the model shown in Fig.3. The resistors are multiplied by two for the same reason [18].

$$C_{SiN(i)} = \varepsilon_0 \cdot \varepsilon_{SiN} \cdot \frac{A_{(i)}}{t_{SiN}} \quad (3)$$

$$C_{SiO2(i)} = \varepsilon_0 \cdot \varepsilon_{SiO2} \cdot \frac{A_{(i)}}{t_{SiO2}} \quad (4)$$

$$C_{S.AlGaN} = \frac{2 \cdot \varepsilon_0 \cdot \varepsilon_{AlGaN} \cdot A_{(i)}}{2 \cdot t_{AlGaN} + \sqrt{v} - \sqrt{4 \cdot t_{AlGaN}^2 + v}} \quad (5)$$

$$R_{S.AlGaN(i)} = \frac{\rho_{AlGaN} \cdot \varepsilon_0 \cdot \varepsilon_{AlGaN}}{C_{S.AlGaN(i)}} \quad (6)$$

B. INPUT/OUTPUT STRIPS AND UNDERPASS BLOCK MODELLING

This model also takes into account the resistance of the input and output strips of metal (R_{IS} and R_{OS}) used to connect the inductor, as well as the resistance of the underpass of the inductor (R_U), which is implemented in the MET1 layer, as stated above. These values can be calculated using (7)–(9), where ρ is the resistivity of the material, l is the length of the strip or underpass and w is the width of said strip/underpass [17]. The effects of the underpass on the substrate are also considered, as shown in Fig.4, where the resistances and capacitances are obtained using (5) and (6).

$$R_{IS} = \frac{\rho_{IN} \cdot l_{IS}}{t_{IN} \cdot w_{IS}} \quad (7)$$

$$R_{OS} = \frac{\rho_{IN} \cdot l_{OS}}{t_{IN} \cdot w_{OS}} \tag{8}$$

$$R_U = \frac{\rho_{MET} \cdot l_U}{t_{MET} \cdot w_U} \tag{9}$$

Another important aspect of this inductor model is that it also considers the parasitic capacitances generated by the coupling between the metal strips of the inductor and the underpass. This effect can be modelled as a simple plane parallel capacitor [19], [20], which is the typical widespread solution. In the case of OMMIC's D01GH process, the SiN and SiO_2 layers found between the IN and MET1 layers (which is used for the underpass) produce capacitive effects due to their dielectric characteristics. Therefore, two series capacitors (C_{PSiN} and C_{PSiO2}) are included to model the overlaps between the IN and MET1 layer for each segment of the inductor. The combination of these two capacitors is calculated for each segment and represented as $C_{UNDERPASS(i)}$ in the model shown in Fig.2. The equations for both capacitors are shown in (10) and (11) [1].

$$C_{PSiN} = \varepsilon_0 \cdot \varepsilon_{SiN} \cdot t_{SiN} \cdot w_{(i)} \cdot w_{UNDERPASS} \tag{10}$$

$$C_{PSiO2} = \varepsilon_0 \cdot \varepsilon_{SiO2} \cdot t_{SiO2} \cdot w_{(i)} \cdot w_{UNDERPASS} \tag{11}$$

C. LATERAL COUPLING MODEL

Finally, the formulation of the C_M and R_M elements that model the lateral coupling in the substrate will also be explained. Although these elements have already been presented in previous publications [12]–[16], in those cases C_M and R_M were obtained via extraction or by using formulae with empirical adjustment factors, whereas in this model they are obtained purely from the dimensions of the inductor and physical properties of the materials that conform the substrate. In order to explain the formulation for C_M and R_M, the area of the lines that conform the inductor (A_{LINES}), the area of the internal hole of the inductor (A_{INT}) and the area occupied by the separation of the turns of the inductor (A_{SEP}) must be calculated. Based on these areas, the total area occupied by the inductor can be defined as shown in (12). The equations for the different areas for an octagonal inductor are shown in (13)-(15). For other types of inductors, such as square ones, the equations for the internal square calculation and separation area must be modified accordingly. In (15), s is the separation between the turns of the inductor and n represents the number of turns of said inductor.

$$A_{TOTAL} = A_{LINES} + A_{INT} + A_{SEP} \tag{12}$$

$$A_{LINES} = \sum_{i=1}^{N} l_{(i)} \cdot w_{(i)} \tag{13}$$

$$A_{SEP} = 2\pi \cdot \left[(n \cdot r_{EXT} \cdot s) - (w_{(1)} \cdot (2n - s - 1)) + 1.5s^2 \right] \tag{14}$$

$$A_{INT} = \pi \cdot r_{INT}^2 \tag{15}$$

When modelling the lateral coupling through the substrate, the main aspects to consider are the capacitance and resistance generated between the edges of the internal hole of the inductor and between the edges of the different turns. This way, it could be theorised that R_M is the series connection of the resistance between the edges of each turn and the resistance between the edges of the internal hole. Therefore, if the equation for the resistance of a three-dimensional conductor (16) is utilised as a reference and modified accordingly, R_M could be calculated as shown in (17), where l_{IND} is the total length of the inductor.

$$R = \rho \cdot \frac{l}{A} = \rho \cdot \frac{l}{w \cdot t} \tag{16}$$

$$R_M = \rho_{Si} \cdot \frac{l_{IND}}{A_{SEP} + A_{INT}} \tag{17}$$

For the calculation of C_M, the equation of a parallel-plate capacitor, shown in (18) was considered [21]. In this case and in a similar fashion to the calculation of R_M, the lateral capacitance can be considered as the series combination of the capacitances that result of the parasitic coupling between the edges of the turns of the inductor in the substrate and between the sides of the inner hole. Since the resulting capacitance in the series connection of capacitors is always determined by the smallest capacitor, in this case C_M is equivalent to the capacitance between the sides of the internal hole of the inductor. The resulting equation for this case is (19), where d_i is the diameter of the internal hole of the inductor.

$$C = \frac{\varepsilon \cdot A}{d} \tag{18}$$

$$C_M = \frac{\varepsilon_0 \cdot \varepsilon_{Si} \cdot A_{INT}}{d_i} \tag{19}$$

III. MODEL VERIFICATION

In order to demonstrate that the developed model can correctly estimate the behaviour inductors of the OMMIC D01GH GaN-on-Si process, seventeen inductors of different shapes (tapered and non-tapered square and octagonal inductors) and sizes were simulated using Keysight Momentum 3D EM Simulator and manufactured. The main characteristics of these inductors are shown in Table 1.

TABLE 1. Physical characteristics of the inductors.

Ind	Inductor type	Tapering [μm/turn]	Ext radius [μm]	No. of turns	Width [μm]	Gap [μm]	Int radius [μm]
L1	Octagonal	2	142	3.5	12	13	50
L2	Octagonal	2	85	2.5	12	14	15
L3	Octagonal	2	114	3.5	17	9	19
L4	Square	No	232	4.5	14	10	18
L5	Square	No	232	4.5	14	10	18
L6	Octagonal	No	70	2.25	14	10	11
L7	Octagonal	No	107	3.5	14	10	16
L8	Square	No	184	3.5	14	10	18
L9	Square	No	112	2	14	10	18
L10	Square	No	232	4.5	14	10	11
L11	Square	No	136	2.25	14	10	5
L12	Square	No	136	2.25	14	10	5
L13	Octagonal	No	142	3.5	14	10	50
L14	Octagonal	No	80	2.5	14	10	16
L15	Octagonal	2	80	2.5	12	14,25	12
L16	Square	2	240	4.5	14	11	18
L17	Octagonal	2*	138.5	3.5	12.5	12,5	50

*First turn of the inductor without tapering.

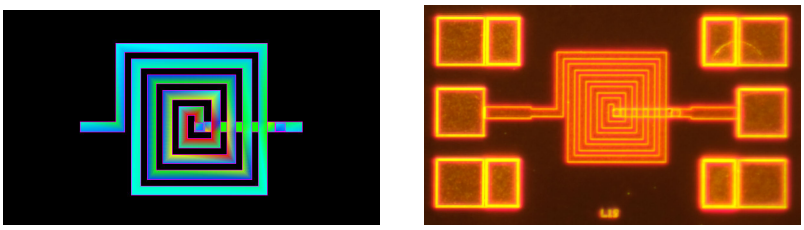

(a) Square inductor (L10)

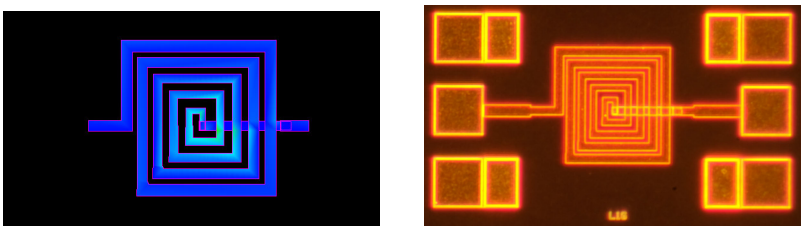

(b) Tapered square inductor (L16)

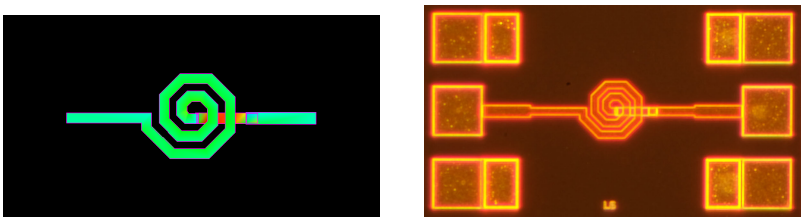

(c) Octagonal inductor (L6)

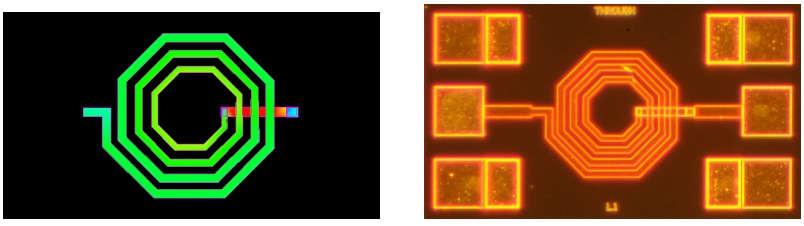

(d) Tapered octagonal inductor (L1)

FIGURE 5. EM simulation and microphotograph of the manufactured inductors.

The inductors were simulated up to 50GHz with a high meshing resolution in order to guarantee that a correct analysis was performed. Fig. 5 shows four of the manufactured inductors (one of each type), as well as current density simulation results for each one at the frequency where the maximum quality factor is reached.

As it can be observed, all the manufactured inductors have input and output GSG pads, so they can be measured directly on-wafer and not be affected by the parasitic effects caused by bonding. The measurements were performed using the Agilent 8720ES S-Parameter Network Analyzer, which permits the measurement of circuits up to 20GHz. All measurement results were obtained by de-embedding the effects of the probes, the GSG pad parasitics and the inductive effects of the metal lines reaching to and from the inductors by using open, short and thru structures that were on the same die as the inductors. Fig. 6 shows the comparison between the EM simulations, the measurements and the developed model for the four inductors shown in Fig. 5. Additionally, Table 2 shows the model parameters for the four inductors shown in Fig. 5.

From the results shown in Fig. 6, it can be observed that the developed model provides excellent results for the estimation of the inductance, most of the times delivering a more accurate result than the EM simulation, both in magnitude and frequency response. The quality factor results, however, show more variability. In some cases, the model is not as precise as the EM simulation result at low frequencies for the octagonal inductors. However, for the other types of inductors, the model matches or improves the results of the EM simulations.

In order to have a more analytical view of the results and perform a more detailed analysis, Table 3 has been filled out. In this table, the measured results for the inductance and

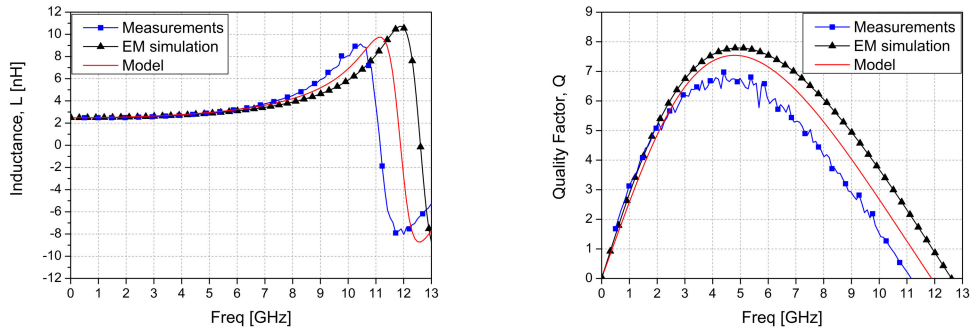

(a) Square inductor (L10)

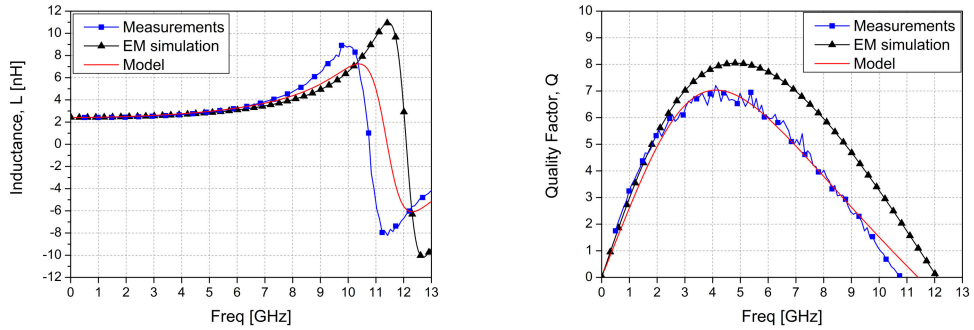

(b) Tapered square inductor (L16)

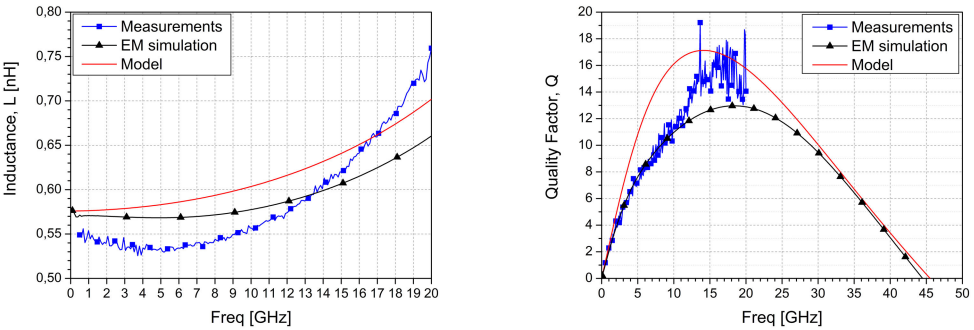

(c) Octagonal inductor (L6)

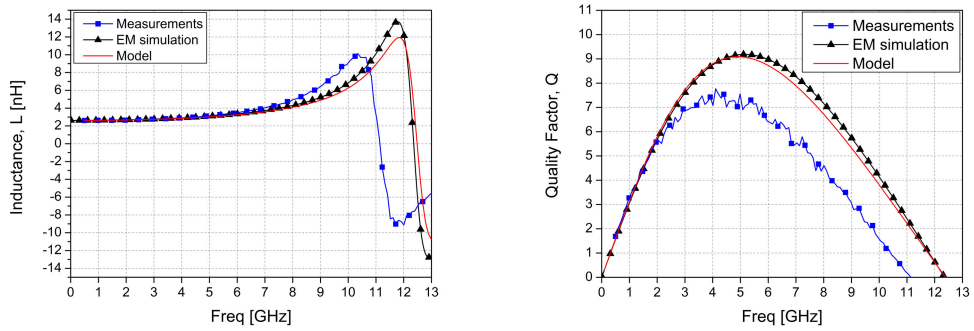

(d) Tapered octagonal inductor (L1)

FIGURE 6. Comparison between the model, EM and simulation results for each inductor shown in Fig. 5.

quality factor have been compared with the results obtained in the EM simulations and with the model presented in this paper. To perform this comparison, the results have been compared at the frequency at which the maximum measured (MM) quality factor (f_{QMM}) is obtained. This way, it can be verified whether the model is valid at a critical point

TABLE 2. Model parameters for the inductors shown in Fig. 5.

	Inductors				
Parameter	L10	L16	L6	L1	Units
L_{DC}	2.482	2.418	0.576	2.627	nH
$R_{SKIN(i)}$	Frequency-dependant				Ohm
$R_{INPUTSTRIP}$	0.0937	0.0859	0.2004	0.0599	Ohm
$R_{OUTPUTSTRIP}$	0.0404	0.0455	0.1349	0.0026	Ohm
$C_{SiN(i)}$	2.527 4.045 2.991 1.937 0.878	3.306 4.165 3.228 2.044 0.643	8.123 1.073 0.348	2.217 3.699 3.699 2.821	pF
$C_{SiO2(i)}$	336.1 537.9 397.7 257.6 116.8	439.6 553.9 429.3 271.7 85.44	108 142.7 46.34	294.8 491.9 491.9 375.1	fF
$R_{S.AlGaN(i)}$	296.5 187.1 251.5 384.3 826.4	228 181.8 233.4 364.9 1114	890.5 681.4 1986	336.9 204.2 204.2 266.3	kOhm
$R_{S.Inter(i)}$	7.584 4.761 6.42 9.862 21.487	5.815 4.625 5.953 9.356 29.173	23.193 17.65 52.911	8.632 5.202 5.202 6.803	Ohm
$R_{S.Si(i)}$	155.4 118.8 141.3 180.3 277.6	133.4 116.8 135.3 175.1 327.9	289.4 249.2 452.6	167.3 125.1 125.1 146.1	kOhm
$C_{S.AlGaN(i)}$	298.6 473.3 352.1 230.4 107.1	388.3 487.1 379.4 242.7 79.47	99.4 129.9 44.58	262.8 433.5 433.5 332.4	fF
$C_{S.Inter(i)}$	583.7 929.8 689.6 448.9 206	761.4 957.2 743.7 473.2 151.8	190.9 250.8 83.6	512.9 851 851 650.7	fF
$C_{S.Si(i)}$	33.33 43.61 36.66 28.72 18.66	38.82 44.36 38.29 29.59 15.79	17.9 20.78 11.44	30.96 41.41 41.41 35.46	fF
$R_{UNDERPASS}$	0.0489	0.5249	0.2881	0.2658	Ohm
$R_{S.AlGaNU.}$	1.112	1.04	1.835	1.979	MOhm
$R_{S.InterU.}$	29.113	27.173	48.744	52.71	Ohm
$R_{S.SiU.}$	327.587	315.5	432.9	451.7	kOhm
$C_{S.AlGaNU.}$	79.63	85.17	48.3	44.75	fF
$C_{S.InterU.}$	152.1	162.9	90.82	83.99	fF
$C_{S.SiU.}$	15.81	16.42	11.96	11.47	fF
$C_{PSiN(i)}$	1.731 1.731 1.731 1.731	2.225 1.978 1.731 1.484	1.731 2.04	1.731 1.484 1.236	fF
$C_{PSiO2(i)}$	7.006 7.006 7.006 7.006	9.008 8.007 7.006 6.005	7.006 8.257	7.006 6.005 5.004	fF
C_M	1.14	1.14	1.23	7.46	F
R_M	1995	1065.7	3329.3	2327.1	Ohm

of each inductor or not. It must be noted that inductor L5 is a variation of inductor L4, but with an additional metalization layer that was not included in the model. Therefore, this inductor and its results are not considered in the overall analysis.

The results shown in the table demonstrate that the model can correctly predict the inductance of the manufactured inductors, showing a maximum positive error of 9.57% when compared to the measured value at f_{QMM}. This error is lower than the maximum positive one obtained in the EM simulations, 12.24% for the same inductor (L15). In general, it can be observed that the results are better for the model, although the results are better for the EM simulation for the case of the non-tapered and tapered square inductors. However, the results of the inductance estimation are evenly matched for both the model and the EM simulations. Based on these results, it can be stated that the model can correctly estimate the inductance of the four types of inductors that have been tested.

Regarding the quality factor, the results are worse than the ones obtained for the inductance, as observed in Fig. 5 and Table 3. In this case, the maximum relative error of the model is obtained for inductor L13, with a result of -37.93%. For the same inductor, the EM simulation relative error is -17.59%, which is a far better estimation. However, if the results are analysed for each type of inductor, the error results of the model are in line with the ones obtained for the EM simulations. Even though the relative errors of the quality factor are greater for both the model and the EM simulation of the inductors, some of this deviation may be due to process variability.

After careful analysis of the discrepancies between the measurements and the results of the model and the EM simulation, it could be articulated that the model provides a better estimation of the inductance and quality factor than the EM simulation for most cases. In fact, the root mean square (RMS) error of all samples for the inductance is practically the same for the model (0.0565) than for the EM simulation (0.0544). The RMS error of the quality factor of all samples is a bit lower for the model (2.2727) than for the EM simulation (2.4776). Based on these results, it could be stated that this model could be utilised to estimate the inductance and quality factor of an inductor manufactured with the D01GH GaN process and, possibly, other processes, both with and without high-resistivity substrates.

IV. CONCLUSION

This paper presents an accurate analytical model for tapered and non-tapered square and octagonal inductors. In this case, the model has been verified by applying it to OMMIC's D01GH GaN process, a novel process that has a high resistivity substrate. A comparison between the measurements of 17 manufactured inductors, their model and their EM simulations was carried out to determine the validity of the model. The results show that the model achieves low error values when compared to the measurement results. These errors are very similar to the ones obtained when comparing the EM simulations and the measurements. This proves that the model is valid and properly estimates the inductance and quality factor of the manufactured inductors. In light of these

TABLE 3. Quality factor, inductance and relative error results for the measurements, EM simulations and model of all inductors.

Ind.	Q_{MM}	f_{QMM} [GHz]	Q_{EM} @f_{QMM}	Q_{Model} @f_{QMM}	Q_{EM} Rel err [%]	Q_{Model} Rel Err [%]	L_{Meas} @f_{QMM} [nH]	L_{EM} @f_{QMM} [nH]	L_{Model} @f_{QMM} [nH]	L_{EM} Rel err [%]	L_{Model} Rel err [%]
L1	9.185	4.9	8.825	8.86	3.92	3.54	2.921	2.917	2.909	0.14	0.41
L2	14.908	14.93	12.836	14.33	13.90	3.88	1.045	0.939	0.947	10.14	9.38
L3	9.853	7.228	10.11	1.865	-2.61	-10.27	1.751	1.721	1.761	1.71	-0.57
L4	6.852	4.9	7.677	7.606	-12.04	-11.00	2.862	2.822	2.891	1.40	-1.01
L5	7.785	4.9	9.236	NA	-18.64	NA	2.789	2.725	NA	2.29	NA
L6	17.888	17.3	12.931	16.687	27.71	6.71	0.674	0.628	0.665	6.82	1.34
L7	9.576	6.545	9.942	12.927	-3.82	-34.99	1.695	1.682	1.709	0.77	-0.83
L8	8.736	7.228	8.958	10.245	-2.54	-17.27	1.5	1.536	1.595	-2.40	-6.33
L9	16.8	17.27	12.306	12.816	26.75	23.71	0.584	0.57	0.622	2.40	-6.51
L10	6.977	4.4	7.722	7.498	-10.68	-7.47	2.778	2.771	2.834	0.25	-2.02
L11	14.272	14.93	10.853	10.667	23.96	25.26	0.887	0.826	0.89	6.88	-0.34
L12	15.156	16	11.709	11.489	22.74	24.20	0.718	0.684	0.747	4.74	-4.04
L13	8.046	4.595	9.461	11.097	-17.59	-37.92	3.076	3.023	3.008	1.72	2.21
L14	14.22	14.25	12.204	14.351	14.18	-0.92	1	0.93	0.957	7.00	4.30
L15	16.232	15.9	11.937	13.217	26.46	18.57	0.899	0.789	0.813	12.24	9.57
L16	7.207	4.107	7.896	7.034	-9.56	2.4	2.694	2.685	2.772	0.33	-2.90
L17	7.724	4.595	9.461	9.875	-22.49	-27.85	3.085	3.023	3.009	2.01	2.46

results, it can be stated that the developed model can be applied for the estimation of the characteristics of an inductor on a GaN on Si process like the D01GH process developed by OMMIC. Further analyses on other technologies will be performed in the future to check if this model can be extended to other processes.

REFERENCES

[1] J. R. Sendra, J. del Pino, A. Hernández, B. Gonzalez, J. Garcia, A. Garcia-Alonso, and A. Nunez, "Integrated inductors modeling for library development and layout generation," *Analog Integr. Circuits Signal Process*, vol. 35, nos. 2–3, pp. 121–132, May 2003, doi: 10.1023/A:1024122430963.

[2] F. M. Rotella, V. Blaschke, and D. Howard, "A broad-band scalable lumped-element inductor model using analytic expressions to incorporate skin effect, substrate loss, and proximity effect," in *IEDM Tech. Dig.*, San Francisco, CA, USA, Dec. 2003, pp. 471–474, doi: 10.1109/IEDM.2002.1175881.

[3] J. Gil and H. Shin, "Simple wide-band on-chip inductor model for silicon-based RF ICs," in *Int. Conf. Simul. Semiconductor Processes Devices (SISPAD)*, Boston, MA, USA, Sep. 2003, pp. 35–38, doi: 10.1109/SISPAD.2003.1233631.

[4] S. S. Mohan, M. del Mar Hershenson, S. P. Boyd, and T. H. Lee, "Simple accurate expressions for planar spiral inductances," *IEEE J. Solid-State Circuits*, vol. 34, no. 10, pp. 1419–1424, Oct. 1999, doi: 10.1109/4.792620.

[5] J. M. Lopez-Villegas, J. Samitier, C. Cane, P. Losantos, and J. Bausells, "Improvement of the quality factor of RF integrated inductors by layout optimization," *IEEE Trans. Microw. Theory Techn.*, vol. 48, no. 1, pp. 76–83, Jan. 2000, doi: 10.1109/22.817474.

[6] V. N. R. Vanukuru and A. Chakravorty, "High-Q characteristics of variable width inductors with reverse excitation," *IEEE Trans. Electron Devices*, vol. 61, no. 9, pp. 3350–3354, Sep. 2014, doi: 10.1109/TED.2014.2340901.

[7] V. N. R. Vanukuru, "High-*Q* inductors utilizing thick metals and dense-tapered spirals," *IEEE Trans. Electron Devices*, vol. 62, no. 9, pp. 3095–3099, Sep. 2015, doi: 10.1109/TED.2015.2458772.

[8] F. Passos, M. H. Fino, and E. R. Moreno, "Fully analytical characterization of the series inductance of tapered integrated inductors," *Int. J. Electron. Telecommun.*, vol. 60, no. 1, pp. 65–69, Mar. 2014, doi: 10.2478/eletel-2014-0007.

[9] J. N. Burghartz and B. Rejaei, "On the design of RF spiral inductors on silicon," *IEEE Trans. Electron Devices*, vol. 50, no. 3, pp. 718–729, Mar. 2003, doi: 10.1109/TED.2003.810474.

[10] R.-J. Chan and J.-C. Guo, "Analysis and modeling of skin and proximity effects for millimeter-wave inductors design in nanoscale Si CMOS," in *Proc. 9th Eur. Microw. Integr. Circuit Conf.*, Rome, Italy, Oct. 2014, pp. 13–16, doi: 10.1109/EuMIC.2014.6997779.

[11] J. Sathyasree, V. Vanukuru, D. Nair, and A. Chakravorty, "Compact modeling of proximity effect in high-Q tapered spiral inductors," *IEEE Electron Device Lett.*, vol. 39, no. 4, pp. 588–590, Apr. 2018, doi: 10.1109/LED.2018.2809787.

[12] J. Sathyasree, V. Vanukuru, D. R. Nair, and A. Chakravorty, "A substrate model for on-chip tapered spiral inductors with forward and reverse excitations," *IEEE Trans. Electron Devices*, vol. 66, no. 1, pp. 802–805, Jan. 2019, doi: 10.1109/TED.2018.2873796.

[13] F. Y. Huang, J. X. Lu, D. M. Jiang, X. C. Wang, and N. Jiang, "A novel analytical approach to parameter extraction for on-chip spiral inductors taking into account high-order parasitic effect," *Solid-State Electron.*, vol. 50, nos. 9–10, pp. 1557–1562, Sep. 2006, doi: 10.1016/j.sse.2006.07.018.

[14] F. Huang, J. Lu, Y. Zhu, N. Jiang, X. Wang, and Y. Chi, "Effect of substrate parasitic inductance on silicon-based transmission lines and on-chip inductors," *IEEE Electron Device Lett.*, vol. 28, no. 11, pp. 1025–1028, Nov. 2007, doi: 10.1109/LED.2007.906800.

[15] A. O. Adan, M. Fukumi, K. Higashi, T. Suyama, M. Miyamoto, and M. Hayashi, "Electromagnetic coupling effects in RFCMOS circuits," in *IEEE MTT-S Int. Microw. Symp. Dig.*, Seattle, WA, USA, vol. 1, Jun. 2002, pp. 39–42, doi: 10.1109/MWSYM.2002.1011553.

[16] J. Zheng, Y.-C. Hahm, V. K. Tripathi, and A. Weisshaar, "CAD-oriented equivalent-circuit modeling of on-chip interconnects on lossy silicon substrate," *IEEE Trans. Microw. Theory Techn.*, vol. 48, no. 9, pp. 1443–1451, Sep. 2000, doi: 10.1109/22.868993.

[17] A. Goni, J. del Pino, B. Gonzalez, and A. Hernandez, "An analytical model of electric substrate losses for planar spiral inductors on silicon," *IEEE Trans. Electron Devices*, vol. 54, no. 3, pp. 546–553, Mar. 2007, doi: 10.1109/TED.2006.890366.

[18] Y. Cao, R. A. Groves, X. Huang, N. D. Zamdmer, J. O. Plouchart, R. A. Wachnik, T. J. King, and C. Hu, "Frequency-independent equivalent-circuit model for on-chip spiral inductors," *IEEE J. Solid-State Circuits*, vol. 38, no. 3, pp. 419–426, Mar. 2003, doi: 10.1109/TED.2003.810474.

[19] T. H. Lee, *The Design of CMOS RF Integrated Circuits,* 2nd ed. New York, NY, USA: Cambridge Univ. Press, 2006.

[20] C. P. Yue and S. S. Wong, "Physical modeling of spiral inductors on silicon," *IEEE Trans. Electron Devices*, vol. 47, no. 3, pp. 560–568, Mar. 2000, doi: 10.1109/16.824729.

[21] H. Nishiyama and M. Nakamura, "Form and capacitance of parallel-plate capacitors," *IEEE Trans. Compon., Packag., Manuf. Technol. A*, vol. 17, no. 3, pp. 477–484, Sep. 1994, doi: 10.1109/22.868993.

MARIO SAN MIGUEL MONTESDEOCA received the B.S. degree in telecommunications technologies engineering and the M.Eng. degree in telecommunications engineering from the University of Las Palmas de Gran Canaria, Spain, in 2014 and 2016, respectively, where he is currently pursuing the Ph.D. degree, with his thesis focusing on MMIC design for Ku and Ka band applications for SATCOM.

From 2014 to 2017, he was an Intern with the RFIC Group, Institute for Applied Microelectronics (IUMA), where he designed RFICs (low noise amplifiers, power amplifiers, and passive mixers) for Zigbee applications. Since 2017, he has been working as a RFIC/MMIC Design Engineer with Wireless Innovative MMIC (WIMMIC). He has authored or coauthored ten publications in international journals and conferences and tutorized two B.S. and one M.Sc. theses. His research interests include MMIC design in III-V technologies like GaN on Si or GaAs, and CMOS and BiCMOS RFICs design for SATCOM and 5G applications.

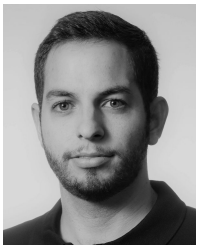

SERGIO MATEOS ANGULO received the B.S. degree in telecommunications technologies engineering and the M.Sc. degree in telecommunications technologies from the University of Las Palmas de Gran Canaria, Spain, in 2015 and 2016, respectively, where he is currently pursuing the Ph.D. degree, with his thesis focusing on the design of radiation hardened-by-design radiofrequency integrated circuits and the analysis of the effects caused by radiation in these circuits.

From 2015 to 2019, he was an Intern with the RFIC Group, Institute for Applied Microelectronics (IUMA), where he designed RFICs (low noise amplifiers, passive mixers, and variable gain amplifiers) for wireless sensor network applications. Since 2019, he has been working as a RFIC/MMIC Design Engineer with Wireless Innovative MMIC (WIMMIC). He has authored or coauthored 13 publications in international journals and conferences. His research interests include MMIC design in III-V technologies like GaN on Si or GaAs, and CMOS and BiCMOS RFICs design for several applications, such as SATCOM and 5G.

DANIEL MAYOR DUARTE received the B.S. degree in telecommunications technologies engineering and the M.Sc. degree in telecommunications technologies from the University of Las Palmas de Gran Canaria, Spain, in 2016 and 2017, respectively, where he is currently pursuing the Ph.D. degree, with his thesis focusing on the design of high power amplifier based on GaAs and GaN technologies.

From 2015 to 2018, he was an Intern with the RFIC Group, Institute for Applied Microelectronics (IUMA), where he designed RFICs (low noise amplifiers, passive mixers, variable gain amplifiers, and filters) for wireless sensor network applications. Since 2018, he has been working as a RFIC/MMIC Design Engineer with Wireless Innovative MMIC (WIMMIC). He has authored or coauthored ten publications in international journals and conferences. His research interests include MMIC design in III-V technologies like GaN on Si or GaAs, and CMOS and BiCMOS RFICs design for several applications, such as SATCOM and 5G.

JAVIER DEL PINO (Member, IEEE) received the B.S., M.S., and Ph.D. degrees in electronics and communication engineering from the University of Las Palmas de Gran Canaria, Spain, in 1996, 1997, and 2002, respectively.

Since 1994, he has been with the Microelectronic Technologic Division, Institute for Applied Microelectronics (IUMA), University of Las Palmas de Gran Canaria. In 1998, he joined as an Associate Professor with the University of Las Palmas de Gran Canaria, from 1998 to 2005, where he has been a Professor since 2005. In 2000 and 2002, he was an Invited Researcher with the Centro de Estudios e Investigaciones Técnicas de Guipúzcoa (CEIT), Spain, and in the Fraunhofer Institute for Integrated Circuits, Germany, respectively. His group has made relevant contributions in the design RFICs and MMICs for different wireless communications standards and technologies. His group also has demonstrated extensive experience in the modeling and optimization of passive components such as varactors and inductors. His group has also helped develop integrated circuits for commercial applications. He has authored or coauthored more than 150 publications in international journals, conferences, and authored the book *Design of Low-Noise Amplifiers for Ultra-Wideband Communications* (McGraw-Hill, 2014). He has graduated six Ph.D. students. He currently leads a group of nine Ph.D. students and postdoctoral Fellows.

JAVIER A. GARCÍA Y GARCÍA (Member, IEEE) received the M.S. degree in physics (specialized in electronics) from the University of Santiago de Compostela, Spain, in 1993, and the Ph.D. degree in electronic engineering from the University of Las Palmas de Gran Canaria (ULPGC), Spain, in 2001.

He was an Invited Researcher with the Centro de Estudios e Investigaciones Técnicas de Guipúzcoa (CEIT), Spain, and the Engineering School (TECNUN), University of Navarra. Since 2003, he has been an Associate Professor with the Department of Electronic Engineering and Control, ULPGC. He is currently a Researcher with the Institute for Applied Microelectronics (IUMA) involved in the Microelectronics Technology Division (TME), ULPGC. He has authored or coauthored more than 60 publications in international journals and conferences. His research interests include timing and power consumption modeling, high-frequency integrated circuits for telecommunications, design, characterization and modeling of integrated inductors and varactors, characterization, and modeling of GaN transistors.

SUNIL L. KHEMCHANDANI (Member, IEEE) received the M.S. and Ph.D. degrees in electronics and communication engineering from the University of Las Palmas de Gran Canaria, Spain, in 2000 and 2007, respectively.

Since 1998, he has been with the Research Institute for Applied Microelectronics, University of Las Palmas de Gran Canaria, where he was working in RFIC for wireless LAN and GaAs IC's for video and image processing. From 2001 to 2003, he was working in INCIDE Canary S.L, where he was involved in the modeling of inductors in CMOS technology, designing of low noise amplifiers for GPS applications, transimpedance amplifiers for SONET/SDH, and phase-locked loops for MMDS. Since 2005, he has been an Associate Professor with the University of Las Palmas de Gran Canaria. He has authored or coauthored more than 90 publications in international journals and conferences and authored the book *Design of Low-Noise Amplifiers for Ultra-Wideband Communications* (McGraw-Hill, 2014). His research interests include RFIC and MMIC circuits for wireless communications and SATCOM.